Ceramics International xxx (xxxx) xxx–xxx

Contents lists available at ScienceDirect

Ceramics International

journal homepage: www.elsevier.com/locate/ceramint

Crystallization-triggered bubbles in glass-ceramics

Oscar Peitl[a], Edgar D. Zanotto[a,*], Klaus Heide[b]

[a] Department of Materials Engineering, Center for Research, Technology and Education in Vitreous Materials, CeRTEV, Federal University of São Carlos, Brazil
[b] Institut für Geowissenschaften - Friedrich-Schiller-Universität Jena, Germany

ARTICLE INFO

Keywords:
Pore
Glass-ceramic
Nucleation
Crystallization
Soda-lime-silica
Lithium silicate

ABSTRACT

Bubbles appear sometimes in glass-ceramics and degrade most properties, especially light transmission and fracture strength. In this work, we deduced microstructural conditions that trigger bubble genesis during crystallization of bubble-free glasses. We related bubble formation to some microstructural parameters in two model glass compositions that exhibit internal crystallization: $1.07Na_2O.2CaO.3SiO_2$ (1.07N2C3S) and $Li_2O.2SiO_2$ (L2S). In this way, we constructed bubble *maps* – experimental diagrams showing a region of bubble nucleation and growth in a crystal size *versus* crystallinity plot. Both glass-ceramics show bubbles having similar geometry that emerge from crystal/liquid interfaces and propagate into the residual liquid. These diagrams show that holes of the order of the crystal size tend to form in glass-ceramics containing a high-volume fraction crystallized (> 50%) and relatively large crystal size (> 10 μm). Mass spectroscopy experiments revealed that bubble formation in the 1.07N2C3S system is caused by O_2. We believe the knowledge generated by this work and resulting *maps* provide a very useful tool for the design of bubble-free glass-ceramics.

1. Introduction

Glass-ceramics (GC) were discovered by S. D. Stookey over 65 years ago. GC research and technology are now mature fields comprising thousands of papers and patents, but many new compositions can still be developed, and several problems remain to be solved [1–4]. Glass-ceramics can be defined as "… *inorganic, non-metallic materials prepared by controlled crystallization of glasses via different processing methods. They contain at least one type of functional crystalline phase and a residual glass. The volume fraction crystallized may vary from ppm to almost 100%*" [5].

Glass-ceramics can be produced in the traditional way - by catalyzed internal crystallization of a monolithic glass article – or by sintering with concurrent surface crystallization of crushed glass powders [1–4]. Sintered glass-ceramics almost always have some residual porosity that degrades most properties, especially optical transparency (due to light scattering) and fracture strength due to the reduction of the volume of solid material and to the introduction of critical-sized defects in the material. However, in some situations, for instance in the development of insulation materials, substrates for catalytic converters, or bioactive scaffolds, pores are desirable and are thus induced on purpose. In this article, we do not deal with residual pores in sintered glass-ceramics; the interested reader is referred to previous studies, *e.g.* Refs. [6–10]. Here we will dwell on bubble generation in traditional glass-ceramics.

One feature that is likely familiar to industrial glass-ceramic researchers, but is not well known by the academic glass research community, is that even traditional glass-ceramics are frequently plagued with bubbles, which appear during crystallization of bubble-free glasses. For instance, George Beall [11] - noted that acmite ($NaFeSi_2O_6$) is a dense phase, approximately 15% denser than its parent glass in which it crystallizes. It is a pyroxene with all the Fe^{3+} in octahedral co-ordination, while the glass has Fe^{3+} as a network former, presumed in tetrahedral co-ordination. This stoichiometric glass-ceramic is "self-nucleating" (or perhaps nucleated by iron oxide) and forms a highly crystalline and fine-grained material with bubbles. Beall always thought those pores were cavitation voids caused by differential shrinkage. However, after reading our short communication [12], he wondered if O_2 solubility was involved, since O_2 could be produced by partial reduction to FeO during melting.

2. Objectives

To the best of our knowledge, the favorable microstructural conditions that lead to crystallization-induced bubbles in traditional (not-sintered) glass-ceramics have only been reported for one particular soda-lime-silica glass-ceramic, (see our preceding communication [12]). In this study, we aim at deepening our understanding of the

* Corresponding author.
E-mail address: dedz@ufscar.br (E.D. Zanotto).
URL: http://www.certev.ufscar.br (E.D. Zanotto).

https://doi.org/10.1016/j.ceramint.2020.06.011
Received 21 April 2020; Received in revised form 31 May 2020; Accepted 1 June 2020

microstructural conditions and causes of (unwanted) bubbles that sometimes form during glass crystallization. The two main mechanisms of formation of pores or bubbles in traditional glass-ceramics are: i) large density misfits between parent glass and crystal phases (cavitation pores); and ii) liberation of dissolved gases induced by crystallization at the crystal/liquid front (bubbles). Here we collect and discuss results about this second mechanism. Using a soda-calcia-silica composition (preliminarily reported in Ref. [12]) and a lithium disilicate glass-ceramic as examples, we constructed experimental *bubble maps*, *i.e.,* bubble-free *versus* bubble-containing zones in crystal size -crystallized fraction plots, and then analyzed and discussed a possible cause of bubble formation in the soda-calcia-silica glass-ceramic.

2.1. Examples of previous studies

We believe the existing knowledge about crystallization-induced bubble creation in traditional glass-ceramics may be hidden as an industrial secret. It is a fact that this type of defect sometimes appears in glass-ceramics, but has been (mostly) neglected by academic researchers, who often report typical phrases such as "*the glass-ceramic microstructure consists of … crystal phases, a residual glass, and some bubbles.*" but rarely try to search for the microstructural conditions that cause them.

As an example of the density misfit mechanism, in one of the few reports dedicated, Fokin et al. [13] studied the generation of pores in a small (mm) piece of a diopside ($CaO.MgO.2SiO_2$) glass, which was enclosed by a rigid crystalline surface layer formed by thermal treatment. The formation of the crystalline layer began after heat treatment of the glass (2.87 g/cm^3) with nucleation and growth of dense (3.27 g/cm^3) diopside crystals on the sample surface. Due to this large density misfit, formation of the rigid crystalline layer stretched the encapsulated liquid and finally led to the birth of a single central "cavitation" pore inside the glass particle, which rapidly grew to a certain size that eliminated the generated elastic stress reducing the driving force for new pore formation. Because the densities of most parent glasses differ from those of the newly born crystals, the findings of ref. [13] are significant for the development of sintered glass–ceramics that undergo surface crystallization.

Turning back to the focus of this article, crystallization-triggered bubbles in traditional (non-sintered) glass-ceramics, in a recent study, Serbena et al. [14] reported on the evolution of crystallization of a stoichiometric lithium disilicate glass, from the parent glass up to the fully crystallized material. They observed the formation of bubbles starting at approximately 65% crystallinity and crystal size > 10 μm, which reached 5% of the sample volume for the 100% crystalline glass-ceramic. They demonstrated that these bubbles reduced the mechanical properties of their glass-ceramic. However, following most authors, they did not divert their research to find out the causes leading to bubble genesis.

In fact, only a few studies, e.g. Ref. [15–19], have reported on bubble nucleation triggered by crystallization. Among these, Akatsuka et al. [15] analyzed the cause of bubble formation in more depth in a surface crystallized $Na_2MnP_2O_7$ glass and found that H_2O was the primary source of bubbles. Another interesting case is SiO_2–B_2O_3–P_2O_5, especially along the SiO_2-BPO_4 join, where so-called "gas ceramics" were found, based on bubbles of hydrogen [1,11]. In this case, as crystalline BPO_4 is nucleated and crystallizes, H_2 bubbles form. To produce these microfoams, the phosphate must be batched with ammonium phosphate, which is the source of hydrogen [11]. However, the microstructural conditions that are favorable for bubble formation were not studied in any of these papers.

In this work, we extend an experimental study of crystallization induced bubbles in a soda-lime-silica glass-ceramic, reported in Ref [12], and complement that work with a lithium disilicate glass, using a series of specially designed thermal treatments that produced a systematic variation of their microstructures in terms of crystallized volume fraction and crystal size. We also constructed a bubble generation "map" in a crystal size *versus* crystallinity diagram for the LS2. The idea was to confirm the results previously obtained for the SLS system. Moreover, using a mass spectroscopy technique, we wanted to determine the nature of the gas trapped in the pores of the soda-lime-silica glass-ceramic.

3. Materials and methods

To produce the desired $1.07Na_2O.2CaO.3SiO_2$ glass (that shows copious internal nucleation), we used Na_2CO_3 (99.8%) and $CaCO_3$ (99.9%), both from Merck, USA, and crushed selected quartz crystals (99.9% SiO_2) from Vitrovita, Brazil. After weighing proper amounts, these chemicals were placed into a powerful planetary mixer for 2 h, then melted at 1300–1360 °C in a platinum crucible in an electric furnace, poured 3 times, crushed, re-melted, and finally cast into a cylindrical graphite mold of 8 mm in diameter and 35 mm in length. The glass samples were then subjected to an annealing treatment at 550 °C, where they were held for 1h and slowly cooled. Finally, disk specimens were cut into approximately 3 mm thick pieces with a diamond disk cutter at low speed, and a chemical analysis was performed by X-ray fluorescence (Table 1 in the Appendix).

The $Li_2O.2SiO_2$ (L2S) batch was prepared with the same technique adopted for the 1.07N2C3S, using Li_2CO_3 (99.9%) from Aldrich, and quartz sand (99.9% SiO_2) from Vitrovita, melted at 1200–1250 °C for 2h in a platinum crucible, poured 3 times, crushed, cast into a graphite mold, and annealed at 458 °C for 1h. We then made a thorough microstructural study with the soda-lime-silica system and a limited study with the L2S glass, to confirm (or not) the most critical topic of this research work, i.e., crystallization-induced bubbles as a function of microstructural parameters of glass-ceramics.

To determine the glass transition and crystallization temperatures of the soda-lime glass, we performed a DSC analysis using a Netzsch equipment, model 400 at 10 °C/min with 15 mg of glass. The resulting T_g = 575 °C and the onset crystallization, T_x, was 708 °C, as shown in Fig. 1. Hence, above 775 °C, this glass is substantially crystallized.

To determine the crystal nucleation kinetics at various temperatures, we used double-stage heat treatments (see table in the Appendix). The micrographs were taken using an optical microscope Jenamed, Carl Zeiss Jena, Germany. The number of crystals per unit area was determined by optical microscopy and analyzed as a function of the nucleation time at different temperatures. Using reflected light optical microscopy, we obtained the number of crystals per unit area, N_S, after

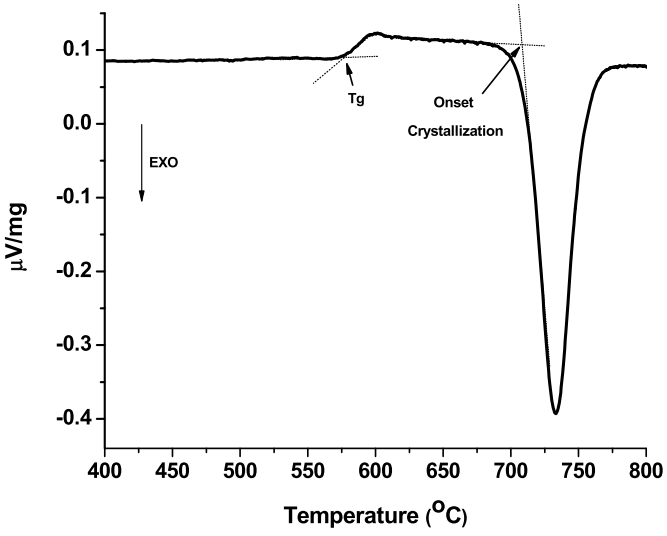

Fig. 1. a – DSC trace of the 1.07N2C3S glass showing the glass transition temperature, T_g, and the crystallization peak, T_x.

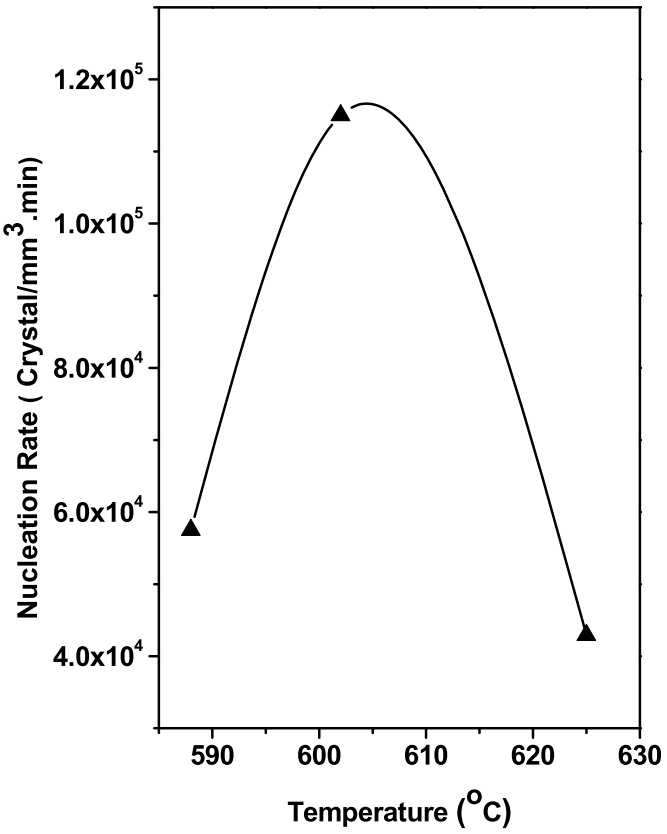

Fig. 2. Estimated nucleation rates of the 1.07N2C3S glass.

counting approximately 300 crystals per heat treatment time and temperature. The average number of crystals per unit volume, N_V, was then calculated by Equation (1).

$$N_V = N_S . Z . F, \quad (1)$$

where $Z = \Sigma_i(1/d_i)/n$, d is the crystal diameter as measured in the sample cross session, and $\underline{n}$ the number of measured crystals per micrograph. The form factor, *F*, depends on the geometry of the crystals; it is 1 to for cubic crystals and $2/\pi$ for spherical particles [20]. Determination of the volume fraction crystallized was made by optical microscopy using the ImageJ software.

For the determination of gases dissolved in the soda-lime-silica glass, powdered samples of about 20 mg of the $1.07Na_2O.2CaO.3SiO_2$, with particle sizes between 400 and 630 μm, were used. A Mettler vacuum extraction equipment, which allowed the simultaneous analysis of several different chemical species (shown in Table 3 Supplementary materials) was employed.

4. Results and discussion

Fig. 2 shows the estimated nucleation rates obtained.

The crystal growth rates were determined following a similar method used to estimate the nucleation rates. After heat treatment at a given nucleation temperature, T_N, for time t_n, which was designed to produce only a small number of crystalline nuclei, they were developed at a temperature T_C for various times t_c. The growth rates were then determined from the slopes of crystal size *versus* time plots at 675 °C and 700 °C. The results are shown in Fig. 3. The positive intercepts in the y-axes are due to pre-existing crystals that nucleated during cooling the melt into the mold, or during the heating path of the samples (that crossed the nucleation curves) to the development temperature.

These nucleation and growth curves were used for designing several microstructures used to construct the *bubble map*. A summary of the

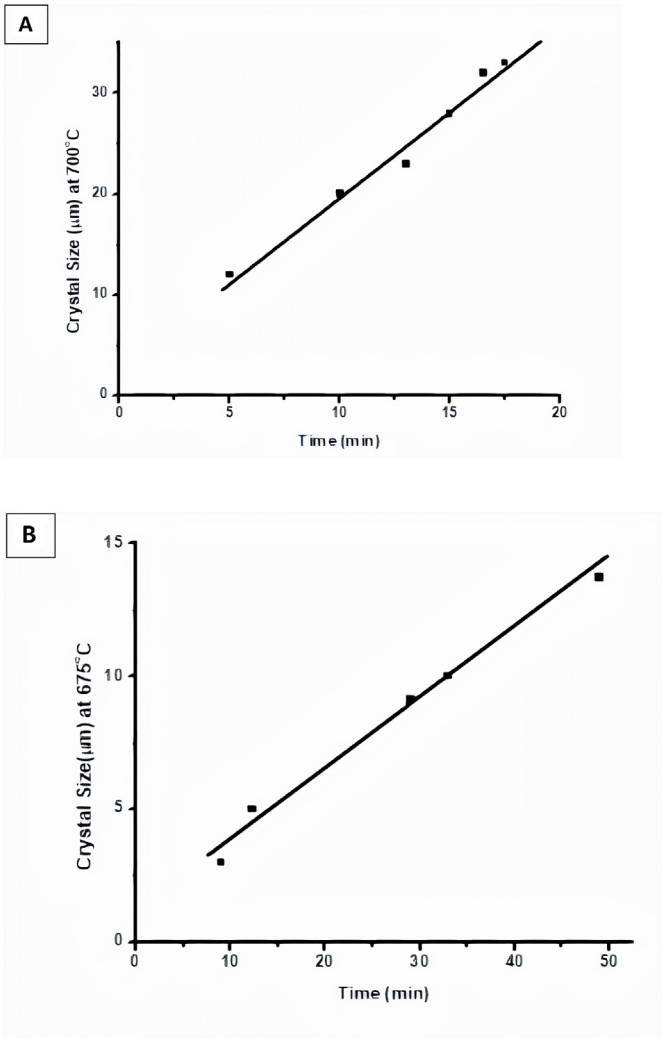

Fig. 3. Crystal growth plots at 700 °C (A) and 675 °C (B) for glass 1.07N2C3S.

heat treatments applied to produce various microstructures with different crystallized fractions and crystal sizes is given in Table 2 (Appendix). We used the largest crystal sizes to plot the *maps*.

Fig. 4 shows examples of the bubble structure existing in a partially crystallized glass-ceramic. We used two microscopy methods for the same sample region and magnification: Fig. 4A was obtained with transmitted light at low magnification using unpolished specimens to highlight the bubble distribution in the glass-ceramic interior. Fig. 4B was obtained with reflected light, and shows cubic crystals, some surface bubbles and their shadows underneath the surface. Fig. 4C was obtained with transmitted light and highlighted an interconnected bubble. It is clear that these bubbles are immersed in the residual glass. Therefore, they emerged and grew in the liquid phase during crystallization. The shadows in these micrographs are due to the interconnected shape assumed by the bubbles, which are not separated spheres, as commonly observed in regular glasses. In Fig. 4C, the same crystals as Fig. 4B can be observed, which are poorly defined in the transmitted light mode.

Regarding the case of pure surface crystallization, the crystal nucleation rates on glass surfaces are greatly enhanced by defects, dust, cracks, and flaws [21,22], hence sample surfaces normally fully crystallize during the crystal growth treatment, when the interior still remains with a low crystallized volume fraction. With the evolution of crystallization towards the sample center, a degassing effect (to be described later in this article) starts forming bubbles, e.g. Ref. [18,19]. Thus, it is important to observe that these bubbles in Fig. 4 are not

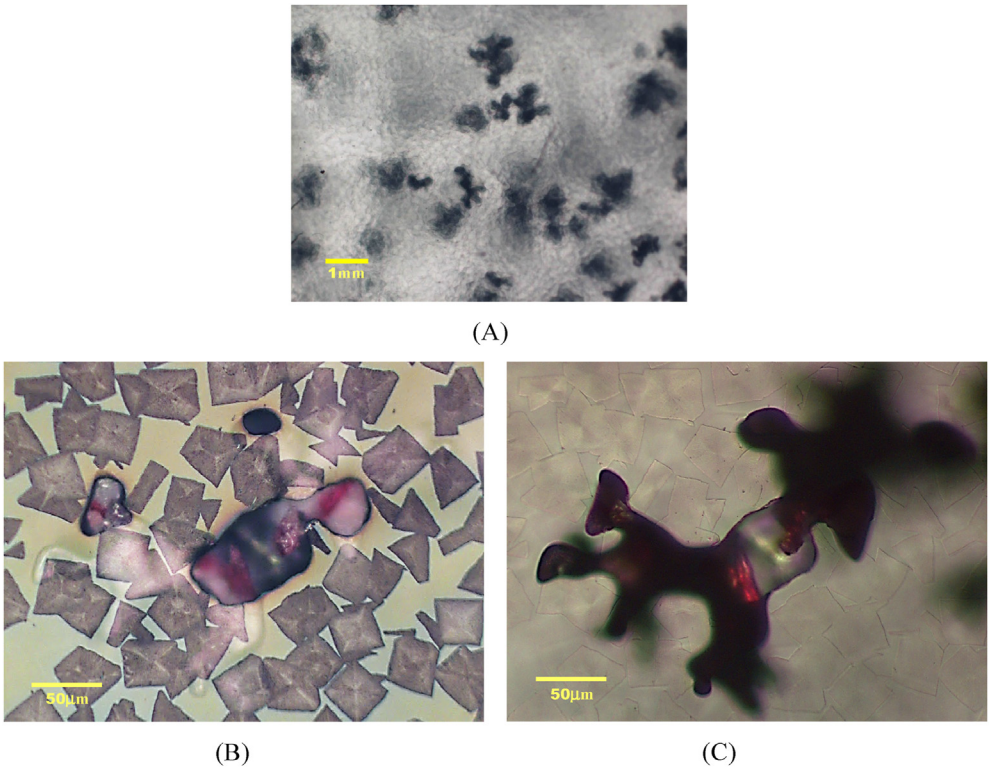

Fig. 4. Optical micrographs of the 1.07N2C3S glass-ceramic showing a sample with bubbles (black regions). A) Unpolished sample probed by transmitted light at low magnification showing dispersed bubbles within the glass interior; B) polished, etched specimen with crystals and bubble shadows seen by reflected light, and C) micrograph obtained in transmitted light mode. Micrograph 4C was obtained from a polished surface with cerium oxide (1 µm) after etching with a diluted solution of HF (0.1%) + HCl (0.05%). Figures B and C are reprinted from the Amer. Cer. Soc. Bulletin [12], where they are printed in color. (For interpretation of the references to color in this figure legend, the reader is referred to the Web version of this article.)

resting on the sample surface. Instead they are located in the sample's interior, among many crystals (these are cross-sections).

Fig. 5 shows the main result of this work for the 1.07N2C3S glass; a bubble "map" of the microstructural conditions necessary to induce or avoid bubble formation in a plot of crystal size *versus* volume fraction crystallized.

This *bubble map* shows that a large volume fraction transformed, in this case, > 50%, leads to bubble generation, suggesting that some dissolved gas super-saturates in the liquid phase and leads to bubble nucleation at the crystal growth front. These bubbles then grow into the residual liquid phase. However, in 3 experiments with crystallized volume fractions up to 95%, no bubble formed if the average crystal size did not exceed 10 µm.

To confirm or not whether a similar bubble *versus* microstructure profile would appear in another glass that undergoes internal nucleation upon adequate heating, we performed the same type of experiments with a stoichiometric lithium disilicate ($Li_2O.2SiO_2$) glass. The glass-ceramics were prepared in the same way described for the 1.07N2C3S composition. The double heat treatments employed were based on the nucleation and crystallization data published by Nascimento et al. [23] for this glass. The nucleation temperatures were in the range of 440–510 °C (T_g ~ 450 °C) with treatment times of 20 min to 15 h. The crystal growth treatments were performed in the temperature range from 550 to 700 °C, with times varying from 1 to 60 min. These treatments were carefully chosen to produce a wide range of microstructures with varying crystal size and volume fraction transformed.

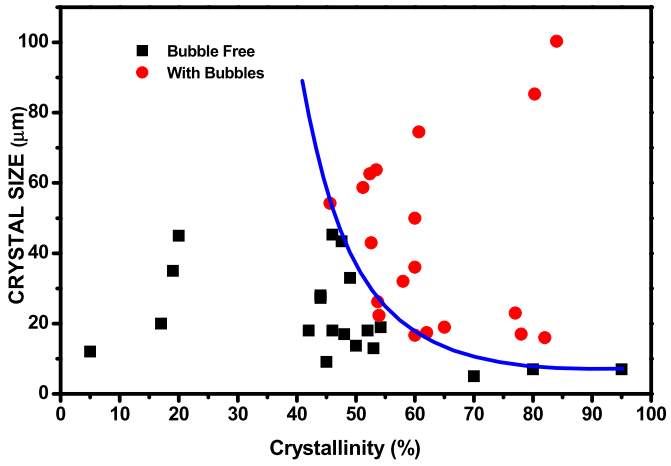

Fig. 5. Bubble map for 1.07N2C3S glass-ceramics with a wide range of microstructures. Largest crystal size versus crystallinity [reprinted from the Amer. Cer. Soc. Bulletin [12]].

Fig. 6 shows micrographs of a glass-ceramic sample after a treatment designed to promote bubbles. For this L2S glass-ceramic, we observe the same bubble shape as for the 1.07N2C3S; snaking in the residual glass phase along the crystals.

For L2S (Fig. 7) we observe the same behavior as for the 1.07N2C3S glass-ceramic. Once more, there is a limiting crystal size, 45 µm in this case, below which it is possible to obtain pore-free fully crystallized glass-ceramics. Although the pore map profiles are similar for both glass compositions, the limiting values of crystal size that lead to porosity are significantly different. The L2S system allows us to reach a greater volume fraction and crystal size than the soda-lime-silica before bubble nucleation is triggered. Therefore, it could be revealing to measure the amount and type of dissolved gases in these materials. We deal with this task in the next session.

4.1. Determination of gases dissolved in the glass soda-lime-silica glass-ceramic

A Mettler vacuum extraction equipment, which allowed the simultaneous analysis of different chemical species, was employed to determine the dissolved glasses in one of these glass-ceramics. The results of these tests for the 1.07N2C3S glass obtained with a heating rate of 5 °C/min under high vacuum extraction are shown in Fig. 8. It is essential to observe that, as shown in the DSC trace of Fig. 1, the glass

Fig. 6. Optical micrograph of a L2S glass-ceramic showing crystals, cracks and bubbles by reflected light (A) and transmitted light (B). The micrograph 6A was taken from a polished surface with cerium oxide (1 µm) etched with a diluted solution of HF (0.1%) + HCl (0.05%).

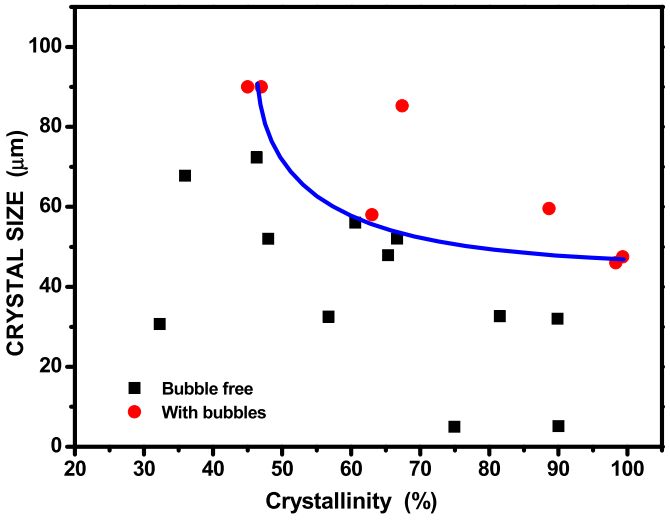

Fig. 7. Bubble map for partially crystallized LS2 glass-ceramics with a wide range of microstructures. Largest crystal size versus crystallinity.

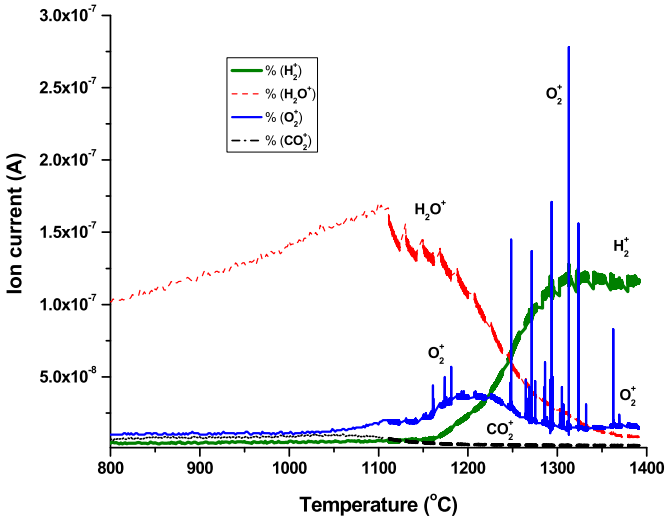

Fig. 8. Gases released from the 1.07N2C3S glass-ceramic (which crystallized substantially at ~800 °C) during high vacuum extraction on the heating path. Each spike indicates a bubble being released. (For interpretation of the references to color in this figure legend, the reader is referred to the Web version of this article)

samples are substantially crystallized at temperatures higher than 800 °C. Therefore, we started to measure gas evolution from such crystallized samples starting at this temperature.

Fig. 8 shows that three main gases are released from the continuously heated glass-ceramic: O_2, H_2O, and some H_2, with significant differences in the respective partial pressures. The other analyzed ions (CO_2, N_2, CO + N_2, NH_4, and SO_2) showed no peaks during the hot vacuum extraction experiment.

It should be stressed that due to the methodology used (automatic and manual) to acquire these data, two regions can be observed. The partial pressure curve of water seems to vary widely around 1100 °C with a discontinuity at this temperature because we changed the operation from the automatic to the manual mode. The automatic mode was only used before numerous blisters appeared in the liquid. To analyze the gas contained in these numerous bubbles, the manual mode of data storage had to be used, which allowed for simultaneous analysis of 10 elements every 100 msec.

Fig. 8 shows differences in water and H_2 release and oxygen bubbling. The oxygen release below 1200 °C is low (only 3 bubbles escaped), whereas, above 1250 °C, oxygen is released by the formation of numerous bubbles, when water release decreased. There is no correlation between the decomposition of Si–OH groups and oxygen. It is known that almost all standard oxide glasses contain from *circa* 10 to 1000 ppm OH^-, hence it is no surprise to see "water" being released at high temperatures under vacuum. In fact, what we call "water" is, in fact, chemically bonded OH^- to silicon, as Si–OH···HO–Si. Fig. 8 shows that the release of water decreases whereas hydrogen release increases with temperature. The release of water and H_2 is continuous, which is a characteristic of a diffusion process. This is because with increasing temperature, above 1150 °C, the formation of H_2 gas from the reaction Si–OH–HO–Si- > **H_2** + 2SiO increases at the expense of H_2O gas, which is controlled by the reaction Si–OH ··· HSiO- > **H_2O** + SiO + Si.

In melting operations under atmospheric conditions, some oxygen (O_2) from the air is always dissolved in the molten mass. However, oxygen release is different; it takes place by blistering. This is typical of a glass refining process without a fining agent. The solubility of oxygen decreases with increasing temperature, and the refining process takes place with the formation and scape of oxygen bubbles. The second hypothesis of oxygen release - redox reactions involving multivalent (impurity) ions, such as iron, cerium, manganese, antimony or arsenic - was discarded because this glass was prepared using pure chemicals that only have a few ppm of these ions. For example, the silica used (primary iron source) has only 20 ppm of iron, and no refining agents were used.

To further test for the presence of gases in the bubbles, a series of glass-ceramic samples containing visible bubbles were prepared by specially designed thermal treatments. They were broken under

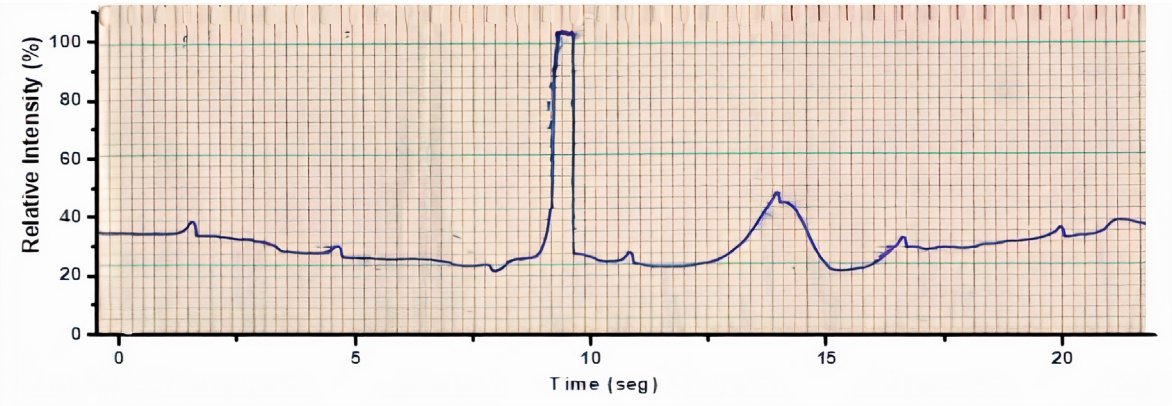

Fig. 9. Photograph of the original mass spectrometry trace showing the relative amount of O_2 (oxygen partial pressure) released on fracturing in three steps a fully crystallized 1.07N2C3S glass-ceramic piece at room temperature. The periodic small bumps refer to noise.

vacuum in several steps at room temperature. The fracture device used was simply a screw that presses the sample against a solid surface causing partial fracture. Each time the screw was rotated a portion of the sample fractured. The fracture released trapped gases from bubbles, which were then analyzed by a coupled mass spectrometer. By setting the mass of each chemical species, this apparatus is capable of analyzing one type of gas per fracture. Hence, several samples were necessary to scan for the most probable gases. Fig. 9 shows the results for the partial pressure of oxygen. None of the other analyzed gases (CO, CO_2, H_2O, N_2 and H_2) were found using this technique.

The first fracture step always produced a larger signal due to O_2 coming out the largest bubbles. However, a portion of the smallest bubbles remained intact. Thus, the subsequent two torsions released gases contained in them. Fig. 9 shows the three O_2 release events. The small peaks that periodically appear in Fig. 9 are due to noise from the old vacuum system. The most intense peak was detected after fracturing the sample the first time and exceeded the plot scale. The second peak appeared after breaking the sample again, and likely originated from a few survivor bubbles existing in the glass-ceramic piece. Finally, a third small peak is also detected in the end, after 21 s. Therefore, oxygen was certainly present in the bubbles of this particular glass-ceramic. We suggest that, since the O_2 solubility in glasses decreases with temperature and, in general, crystals can take less dissolved gases than the liquid phase, the increase in crystallinity in the microstructure likely leads to O_2 supersaturation in the residual liquid and promotes bubble genesis at the crystal/liquid interface [24,25].

We should emphasize that the two techniques employed for gas analysis provide different, complementary information. In the first, gases are released while heating a sample after it partially crystallizes and reaches a temperature where the viscosity of the residual liquid is low enough for vacuum removal of all gases. Therefore, all (or most) gas species that were dissolved in the liquid and crystal phases of the glass-ceramic are removed. On the other hand, in the other method, which works by breaking pre-prepared glass-ceramic pieces containing bubbles at room temperature, under vacuum, only the gases already existing inside the bubbles are released and can be identified. The other gases remain dissolved in the material. Therefore, for this work, the second test was essential to identify the source of the detected residual bubbles.

It is understandable why with increased crystallinity, bubbles are generated and grow into the liquid phase. However, it is still not clear to us the reason why, even with a very high volume transformed fraction, relatively small crystals (apparently) do not trigger bubble formation.

A possible hypothesis, suggested by G. Beall [11], could be that lower growth temperatures used for crystal development of the GC with finer microstructures were related to slower crystal growth rates, which allowed for gas redistribution in the residual liquid. Perhaps the diffusion rate of the dissolved gas in the glass is a smaller function of temperature as compared to the crystal growth rate. If so, this would suggest that lower crystal growth rates, due to growing at lower temperatures, might allow the dissolved gas species to equilibrate more easily throughout the glass and perhaps account for the lack of bubble formation with finer grains. This is a rational hypothesis. However, we found no correlation between growth temperature and bubble generation.

Another reasonable assumption is that by incrementing the interfacial area with decreasing crystal size, dissolved gas is more uniformly dispersed along the crystal/liquid interfaces and the saturation level does not reach the required, critical local saturation concentration to create bubbles. Indeed, the micrographs of Figs. 4 and 6 show that the bubbles are not dispersed homogeneously within the glass phase; they only nucleate in certain regions in the microstructure.

Still another possibility is that for the finest microstructures the generated bubbles are too small to be quickly resolved by optical microscopy? In any case, this question warrants further study. We hope the current results motivate researchers and students to follow up along these lines.

Luckily, however, many (but not all) commercial glass-ceramics contain nano sized crystals and hence, apparently, do not suffer from the bubble problem. Bubble-generation maps might be of great interest to researchers working on bioactive glass-ceramics [26], such as the SLS material studied here, and dental glass-ceramics [1]. These important types of GC have high fracture toughness and strength, and micrometric (not nanosized) crystals, which sometimes lead to bubble formation. Another application relates to crystallizing glasses used for glass-to-metal seals, for which larger crystals are expected. As the crystallization in glass-to-metals seals is usually quick and the crystals are relatively large, there might be a connection to an application with widespread and significant commercial significance [27]. Finally, crystallization generated bubbles could also be relevant in geosciences, e.g., during crystallization of lavas for which such effects are critical towards our understanding of how volcanoes can be so dangerously explosive [28]. This interesting topic certainly warrants further study.

5. Summary and conclusions

For two types of glass-ceramics, we deciphered the microstructural conditions that trigger bubble-induced crystallization, and suggested a mechanism for this type of bubble genesis by constructing *bubble maps* - experimental diagrams showing regions of bubble plagued and bubble-free materials as a function of the percentage crystallinity and largest crystal size. We also analyzed the type of gas in the bubbles of one type of glass-ceramic.

These *maps* show that bubbles tend to nucleate and grow in certain glass-ceramics having relatively high-volume fraction crystallized (> 50%) and relatively large, micrometric crystal size. A possible explanation for this phenomenon is that most crystals can take less dissolved gases than the residual liquid. Hence, increasing crystallinity leads to gas supersaturation in the residual liquid, which promotes bubble nucleation at the crystal/liquid interfaces. Moreover, mass spectroscopy experiments demonstrated that bubble formation in the soda-lime-silica glass-ceramic is due to O_2. We hypothesize that these bubbles are formed due supersaturation of O_2 in the residual liquid as crystallization proceeds leading to gas exsolution.

We believe the knowledge generated by this work, on crystallization-induced bubbles in general, and specifically the proposed bubble *maps,* allow for fine-tuning of heat treatment schedules and may serve as a handy tool for designing and developing bubble-free glass-ceramics.

Acknowledgments

The authors are indebted to the São Paulo Research Foundation, Fapesp, CEPID Process # 2013/007796-3 for the generous funding, and to George Beall and Mark Davis for their valuable suggestions.

Appendix

Table 1
Nominal composition of the soda-lime-silica glass and chemical analysis by X-ray fluorescence (wt%).

Glass 1.07N2C3S	SiO_2 (%)	Na_2O	CaO	Al_2O_3	K_2O	TiO_2
Nominal	50.3	18.5	31.2	#	#	#
Experimental	50.5	18.5	30.8	< 0.02	< 0.01	0.08

Table 2
Range of heat treatments used to construct the *pore map* for the 1.07N2C3S and LS2 glass-ceramics.

	1.07N2C3S		LS2	
	T(°C)	Time (min)	T (°C)	Time (min)
Nucleation	600–630	0-9000	470	5–150
Growth	675–700	5–80	615–630	5–15

Table 3
Ionic species analyzed by mass spectroscopy coupled to a vacuum extraction equipment at high temperatures.

Species	Atomic mass	Species	Atomic mass
H_2^+	2	N_2^+-CO^+	28
N^+	14	O_2^+	32
CH_3^+	15		
H_2O^+	18	CO_2^+	44
		SO_2^+	64

References

[1] W. Holland, G.H. Beall, Glass Ceramic Technology, second ed., John Wiley & Sons, 2012, p. 440.
[2] M.J. Davis, E.D. Zanotto, Glass-ceramics and realization of the unobtainable: property combinations that push the envelope, MRS Bull. 42 (3) (2017) 195–199.
[3] M. Montazerian, S.P. Singh, E.D. Zanotto, An analysis of glass-ceramic research and commercialization, Am. Ceram. Soc. Bull. 94 (4) (2015) 30–35.
[4] E.D. Zanotto, A bright future for glass-ceramics, Am. Ceram. Soc. Bull. 89 (8) (2010) 19–27.
[5] J. Deubener, M. Allix, M.J. Davis, A. Duran, T. Höche, T. Honma, T. Komatsu, S. Krüger, I. Mitra, R. Müller, S. Nakane, M.J. Pascual, J.W.P. Schmelzer, E.D. Zanotto, S. Zhou, Updated definition of glass-ceramics, J. Non-Cryst. Solids 501 (2018) 3–10.
[6] A. Karamanov, M. Pelino, - Induced crystallization porosity and properties of sintered diopside and wollastonite glass-ceramics, J. Eur. Ceram. Soc. 28 (3) (2008) 555–562.
[7] A. Karamanov, M. Pelino, Sinter-crystallisation in the diopside-albite system. Part I. Formation of induced crystallisation porosity, J. Eur. Ceram. Soc. 26 (13) (2006) 2511–2517.
[8] M.O. Prado, C. Fredericci, E.D. Zanotto, Isothermal sintering with concurrent crystallization of polydispersed soda-lime-silica glass beads, J. Non-Cryst. Solids 331 (1–3) (2003) 145–156.
[9] M.O. Prado, C. Fredericci, E.D. Zanotto, Non-isothermal sintering with concurrent crystallization of polydispersed soda-lime-silica glass beads, J. Non-Cryst. Solids 331 (1–3) (2003) 157–167.
[10] M.O. Prado, E.D. Zanotto, Glass sintering with concurrent crystallization, Compt. Rendus Chem. 5 (11) (2002) 773–786.
[11] Beall, G. – Personal Communication (2019).
[12] O. Peitl, E.D. Zanotto, Bubbles – a glass-ceramic plague - Amer, Ceram. Soc. Bull. 98 (4) (2019) 30–33.
[13] V.M. Fokin, A.S. Abyzov, J.W.P. Schmelzer, E.D. Zanotto, Stress induced pore formation and phase selection in a crystallizing stretched glass -, J. Non-Cryst. Solids 356 (33/34) (2010) 1679–1688.
[14] F.C. Serbena, I. Mathias, C.E. Foerster, E.D. Zanotto, Crystallization toughening of a model glass-ceramic -, Acta Mater. 86 (2015) 216–228.
[15] C. Akatsuka, T. Honma, R. Müller, S. Reinsch, S. Tanaka, T. Komatsu, Surface crystallization and gas bubble formation during conventional heat treatment in $Na_2MnP_2O_7$ glass -, J. Non-Cryst. Solids 510 (2019) 36–41.
[16] T. Aboud, Glass ceramization as an alternative production route of forsterite glass-ceramics for possible multipurpose uses -, Adv. Mater. Res. 1043 (2014) 138–144.
[17] J.R. Martinelli, F.F. Sene, C.N. Kamikawachi, C.S.D.M. Partiti, D.R. Cornejo, Synthesis and characterization of glass-ceramic microspheres for thermotherapy, J. Non-Cryst. Solids 356 (44–49) (2010) 2683–2688.
[18] M.O. Prado, C. Fredericci, E.D. Zanotto, Isothermal sintering with concurrent crystallization of polydispersed soda-lime-silica glass beads, J. Non-Cryst. Solids 331 (1–3) (2003) 145–156.
[19] K. Heide, E. Hartmann, Th Stelzner, R. Müller, Degassing of a cordierite glass melt during nucleation and crystallization, Thermochim. Acta 280–281 (1996) 243–250 (special issue).
[20] C.J.R. Gonzalez-Oliver, P.F. James, Crystal nucleation and growth in a $NaO.2CaO.3SiO_2$ glass, J. Non-Cryst. Solids 38/39 (1980) 699–704.
[21] R. Müller, E.D. Zanotto, V.M. Fokin, Surface crystallization of silicate glasses:

nucleation sites and kinetics, J. Non-Cryst. Solids 274 (1) (2000) 208–231.
[22] E.D. - Glass Zanotto, Crystallization Research - a 36-year retrospective. Part II, Methods of study and glass-ceramics, Int. J. Appl. Glass Sci. 4 (2) (2013) 117–124.
[23] M.L.F. Nascimento, V.M. Fokin, E.D. Zanotto, A.S. Abyzov, Dynamic processes in a silicate liquid from above melting to below the glass transition -, J. Chem. Phys. 135 (2011) 1–18.
[24] K. Heide, Gas release from minerals, Minerals as Advanced Materials II, (2012), pp. 25–36 9783642200182.
[25] G. Völksch, K. Heide, Dissolved gases and minor component effects on glass crystallization -, J. Non-Cryst. Solids 219 (1997) 119–127.
[26] M.C. Crovace, M.T. Souza, C.R. Chinaglia, O. Peitl, E.D. Zanotto, Biosilicate® — a multipurpose, highly bioactive glass-ceramic. In vitro, in vivo and clinical trials-, J. Non-Cryst. Solids 432 (2016) 90–110.
[27] P.W. McMillan, Glass Ceramics, Academic Press, 1979, p. 285.
[28] M.C. Davis, Personal Communication, (2019).